Brief Communication : Monitoring active layer dynamic using a lightweight nimble Ground-Penetrating Radar system. A laboratory analog test case.

Emmanuel Léger[1], Albane Saintenoy[1], Mohammed Serhir[3], François Costard[1], and Christophe Grenier[2,†]

[1]Université Paris-Saclay, CNRS, GEOPS, 91405, Orsay, France
[2,†]Laboratoire des Sciences du Climat et de l'Environnement, Université Paris-Saclay,IPSL/LSCE, UMR 8212 CNRS-CEA-UVSQ, Orme des Merisiers, Gif-sur-Yvette Cedex,France. Deceased
[3]Université Paris-Saclay, CentraleSupélec, CNRS, Laboratoire de Génie Electrique et Electronique de Paris, 91192, Gif-sur-Yvette, France

Correspondence: emmanuel.leger@universite-paris-saclay.fr

Abstract. Monitoring active layer dynamic is critical for improving the near surface thermal and hydrological process understanding in the cryosphere. This study presents the laboratory test of a low-cost Ground-Penetrating Radar (GPR) system within a laboratory experiment of active layer freezing and thawing monitoring. The system is an in-house built low power monostatic GPR antenna coupled with a reflectometer piloted by a single board computer, tested prior to field deployment. The correspondence between the frozen front electromagnetic reflection and temperature allowed to test the ability of the system to closely monitor the frozen front/bottom of the active layer reflection.

1 Introduction

The freezing and thawing cycles of frozen material in cryosphere environment are important processes not only for water and temperature redistributions, but are critical for nutrient cycles (Nitrogen and Carbon) and atmosphere gas release. As such, monitoring, non destructively, the seasonal soil freezing and thawing in high latitude contexts has been an extensive topic of interest in cold regions advances. Previous researchers have illustrated the suitability of geophysical methods, especially Ground-Penetrating Radar (GPR) techniques, for monitoring active layer freezing and thawing (Liu and Arcone, 2003; van der Kruk et al., 2009; Jadoon et al., 2015; van der Kruk et al., 2007; Westermann et al., 2010; Steelman and Endres, 2009; Sudakova et al., 2021). Reflection from the permafrost table, or active layer base, were compared in GPR profiles with acquisitions repeated at different times (Westermann et al., 2010; Sudakova et al., 2021). The first 10 cm soil freezing/thawing cycles over 9 days was monitored using a static antenna set of an air-launched off-ground GPR system (Jadoon et al., 2015). With the same steady monitoring approach, common mid-point techniques were used to study electromagnetic wave dispersion and frequency to infer active layer freezing and thawing acting as waveguide (van der Kruk et al., 2009; Steelman and Endres, 2009). As far as we know, no studies were performed using monostatic on-ground antenna monitoring on the same location through time apart a first attempt in laboratory with a commercial antenna system (Saintenoy et al., 2005). Here we present a novel combination of low-cost/-energy nimble GPR mono-static ground-coupled antenna with a reflectometer in conjunction with a small array of
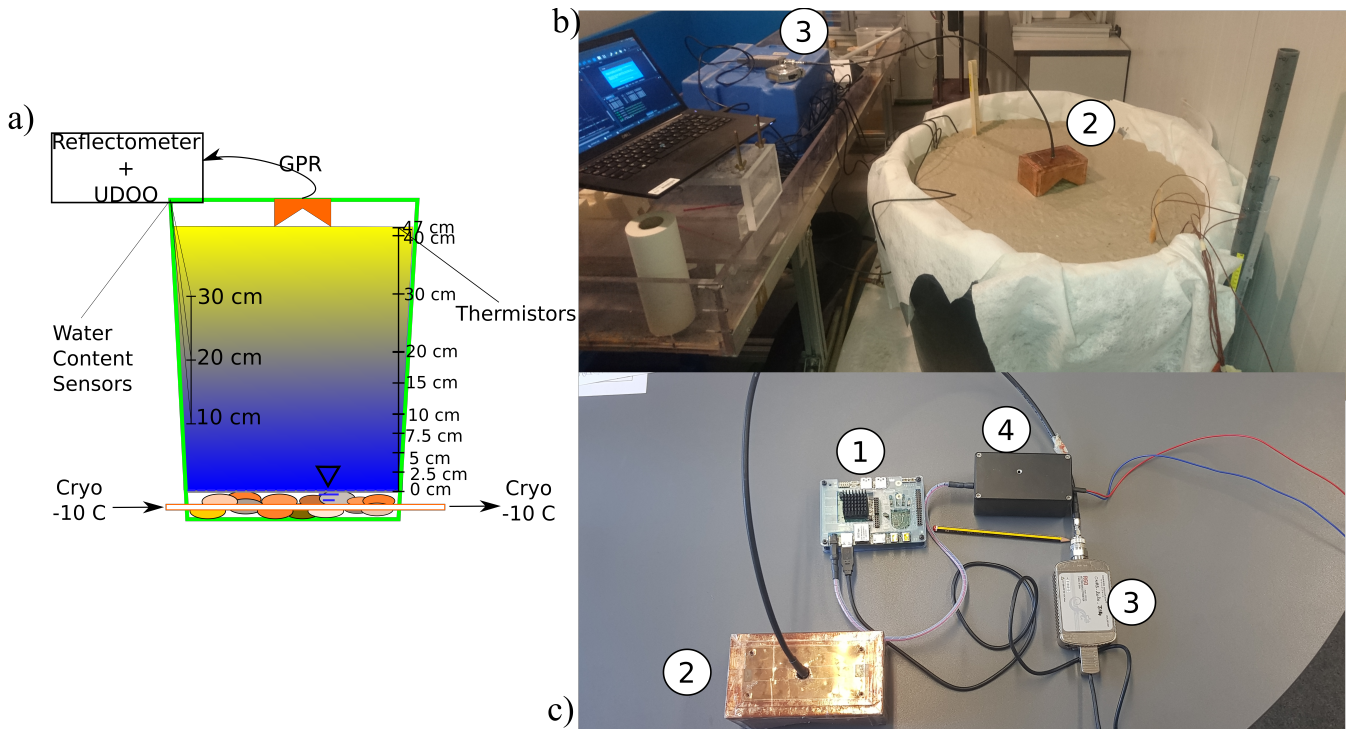
Figure 1. Experimental setup : a) draft of the experiment where volumetric water content sensors are on the left and thermistors on the right side of the draft, the cryogenic fluid is flowing at the bottom of the tank at -10°C; b) picture of the GPR prototype with the antenna (2) and the reflectometer (3) in the cold room, c) picture of the 4 main components of the M-GPR system: UDOO SBC computer (1), butterfly antenna (2), reflectometer (3) and power-supply timer (4) plugged to a 12 V car battery. The pencil gives the scale.

thermal and volumetric water content sensors for monitoring active layer freezing and thawing during laboratory experiments. The study is thought as a first test case on a active layer laboratory analog before near future field deployments.

2 Materials and Methods

2.1 Autonomous Monitoring Ground Penetrating Radar System : M-GPR

The M-GPR system comprises an ultra-wide band antenna designed in the GeePs Laboratory operating in frequency band 0.1 GHz – 6 GHz. The antenna is a fractal-folded complementary bowtie antenna (Liu et al., 2018). It is combined with the R60 Copper Mountain (http://coppermountaintech.com) USB vector network analyzer to measure the reflection coefficient (in this case S_{11}) of antenna placed in front of the area under test (Figure 1). The antenna design has been engineered with fractals in order to enlarge the covered bandwidth. It is enclosed in a shielded cavity to reduce backward radiation and to protect from external electromagnetic perturbations. Inside the cavity, absorbers are placed to prevent the antenna performance degradation while reducing multiple reflections inside the cavity.

The R60 Copper Mountain reflectometer is controlled (via serial USB connection) using an UDOO single board computer (SECO S.P.A.). The board is powered using a stabilized current source (12 V) and a timer (CRONTAB) to allow power/sleep modes for long time monitoring campaign. For the presented results, a stack of 10 traces was performed regularly in time (every 5 minutes) where the real and imaginary part of S_{11} were recorded over 801 points covering the frequency band 0.2 GHz – 5 GHz. The frequency domain measurement data were inverse Fourier transformed to generate time domain radargrams with a time window of 30 ns. The expected dynamic range of measured data can reach up to 90 dB using the R60 Copper Mountain reflectometer and adopting the step frequency technique. In addition, on a 12 V/ 60 Ah battery, the GPR system offers the possibility to monitor during a month with a measurement every 5 minutes including the pre-heating of the reflectometer and a stack of 10 traces. Using the M-GPR system, one can configure the timer to wake-up the UDOO board computer every 12 hours in order to monitor the area under investigation during months.

2.2 Laboratory Modeled Active Layer characteristics

The laboratory-analog active layer was made of Fontainebleau fine sand ($D_{50}= 200$ μm) contained in a cylindrical vase shaped reservoir of 52 cm height and a 84-90 cm diameter, as drafted and depicted in Figures 1-a) and 1-b). At the base of the column, a system of home-made copper pipes was installed and connected to an external cryostat flowing glycol in the copper pipes at -10°C. The freezing copper pipes were surrounded by a gravel layer, used as drainage horizon and spreading the weight of the above sand layer. A thin layer of aluminum foil with multiple holes was placed above the gravel layer to create a strong bottom reflector. A thin geo-textile sheet was set on top of the drainage-freezing layer for preventing the sand to be flushed out and to keep minimal the frost heave according to Henry (1990). The inner-diameter of the cylinder was covered by polystyrene foam blankets all around its inner diameter, to ensure as much as possible radial thermal insulation and keep only the top (atmosphere +1°C) and bottom (copper pipe linked to cryostat) boundaries (-10°C) as open thermal flow conditions.

The cylindrical tank was hydraulically connected to tap water with a buffer reservoir system allowing to set water table at different heights. This system allowed us to properly and incrementally saturate the sand material while compacting it in the reservoir. The sand hydrodynamic parameters, such as the Mualem (1976) - van Genuchten (1980)'s parameters can be found in Léger et al. (2020). A well-proven technique (Costard et al., 2021) was used to create a homogeneous porous medium of more than 400 kg of saturated soil : we manually compacted layers of 10 cm each by maintaining the water level higher than the considered layer and then put them on top of each other until 0.47 m thickness was reached. The sand was packed to a porosity estimated to be 0.39. There might be some small interfaces (thin unconformities), but they remain insignificant (we verified post experimentally when excavating the sand).

The low temperature external atmospheric conditions were set using the cold room facility at the GEOPS laboratory (University Paris Saclay, France) dedicated to the physical modeling in periglacial geomorphology (Costard et al., 2021). The external temperature of the cold room was maintained slightly above +1°C, throughout the freezing phase. For shortening the thawing time length, the thawing phase was performed by shutting down all freezing processes, open the cold room, and equilibrate with ambient temperature in the building ($\approx$ +20°C). As drawn in Figure 1-a), a string of 10 thermistors (PT100 with $\pm$ 0.1 °C) were set from the bottom of the sand layer to the surface at 0, 2.5, 5, 7.5, 10, 15, 20, 30, 40 and 47 centimeters from the

bottom. Complementing these thermal measurements, 3 volumetric water content sensors (Meter Terros 12, metergroup.com) were set diametrically opposed to the thermistors string at 10, 20 and 30 cm from the bottom of the sand layer. In addition to the sensor network, a handheld thermal camera (Flir TG297, Teledyne FLIR LLC) was used to check the thermal isolation continuity of the cylindrical reservoir, notably the thermal insulating polystyrene layer on the curvilinear sides of the reservoir.

2.3 Electromagnetic Wave Velocity As A Function Of Soil Dielectric Properties

The mono-static antenna emits and receives frequency sweep of spherical electromagnetic (EM) waves in response to the reflectometer excitation at different frequencies. The receiving antenna converts the incoming EM fields to electrical digital signals. Following the work of Annan (1999), the velocity of an electromagnetic wave propagating in a non-magnetic soil, with low electrical conductivity, can be approximated by :

$$v = \frac{c}{\sqrt{\varepsilon'}} \,, \tag{1}$$

where ε' denotes the real part of the relative dielectric permittivity and $c = 0.3$ m/ns is the velocity of EM waves in air.

The dielectric permittivity depends on the media component content, such as water, air, minerals and ice content. We used the volumetric mean Complex Refractive Index Model (Birchak et al., 1974), where the relative dielectric permittivity of the porous material, ε_b, is a function of the material porosity, its state of saturation and the respective permittivity of each of its individual constituents. For the thawed water-saturated case, considering no air is entrapped, the Fontainebleau sand medium is bi-phasic composed of water and silica :

$$\varepsilon_b^\gamma = \phi \varepsilon_w^\gamma + (1-\phi)\varepsilon_s^\gamma \,, \tag{2}$$

where ε_w and ε_s are respectively the relative dielectric permittivity of water and of silica, ϕ is the porosity, and γ is an empirical coefficient that depends on soil structure. In this study, we set $\varepsilon_w = 80.1$, $\varepsilon_s = 4.2$, $\phi = 0.39$ and $\gamma = 0.5$ as in Léger et al. (2020). We assumed all media were non conductive and no dispersion effect was taken into account. The frozen case was similar to equation (2) except that the liquid water phase was replaced by its solid phase, considering that no air was entrapped and that no change in porosity was resulting from the freezing phase,

$$\varepsilon_b^\gamma = \phi \varepsilon_i^\gamma + (1-\phi)\varepsilon_s^\gamma \,, \tag{3}$$

where ε_i is the relative dielectric permittivity of ice (set here to 3.1). A transition zone was assumed between these two types of media (frozen/ unfrozen) were coexistence between frozen and thawed media was derived using an empirical freezing curve (the sinus of the ice content percentage in pores decreasing linearly from 100 to 0) without considering any change in porosity through the freezing process. This modeling, despite its simplicity is thought as a first numerical analog to the media aiming to simulate roughly a bottom freezing active layer.

2.4 Electromagnetic modeling

For simulating our M-GPR data we used the open source software GprMax2D (Warren et al., 2016), in two dimensions, as presented in Léger et al. (2020). The EM model was set to 1.2 m wide and 0.6 m high, larger than the real model to avoid

side effects, filled up to 0.47 m with saturated sand following the simplistic permittivity distribution presented in section 2.3. The cell size were 5x5 mm^2, a Perfect Electrical Conductor (PEC) layer was set at the bottom of the sand layer and the model domain sides were padded with 10 cell thick absorbing boundaries. The freezing layer was modeled using the dielectric permittivity distribution (derived from Equation 3) corresponding to a frozen layer increasing from 0.02 m up to 0.3 m with 2 cm step. The GPR antenna was modeled by a Hertzian dipole polarized in the direction perpendicular to the 2D plane model, emitting a Ricker waveform centered on 1.5 GHz. This simplistic EM model was thought as a first try aiming to understand from where the various reflections are coming from during the bottom active layer freezing.

3 Results

We present in detail the results of one experiment while 4 others are available in supplementary materials.

3.1 Temperature and volumetric liquid water content time series

The temperature time series measured during one of the experiments are presented in Figure 2-a). During the equilibrating phase the surface temperature sensor drops the fastest to the constraint cold room temperature (+1°C). The thermal time series exhibit little 8-hour cycles for the shallowest sensor at the surface due to the chamber cryostat defrost cycles, maintaining the cold room at +1 °C. The bottom freezing phase start is symbolized by the blue dashed vertical line at 21:00 on the day 21 corresponding to the zero experimental time. At the base of the sand layer the temperature reaches within few hours the zero-degree isotherm with a typical curtain effect for the sensors close to the cold system (z = 0, 2.5, 5 cm), while almost a day is required for sensors from 20 cm to the top. Near surface and surface sensors (40 cm and Surface) are within the 0°C. Once the 0°C isotherm is crossed, the temperature are following an exponential decrease as expected (Hinzman et al., 1998). The depth-temperature profile derived from the time series presented in 2-c) exhibits the depth of the zero-degree isotherm reaching the ground surface after 60 h from the start of the experiment. Once the freezing phase done, the thawing phase exhibits a fast thawing for the first 30 cm below the surface while it takes more time deeper, with an optimum at 10 cm corresponding to the balance between heat dissipation and proximity to the bottom freezing cold source inertia. The heat dissipation is as well visible on the different evolution of the curve with depth.

The volumetric liquid water content in the column is homogeneous during the equilibrating phase, Figure 2-b), except the 20-cm sensor being a bit lower comparing to the rest of the column, probably due to a mis-calibration or water-unsaturated macro-pore(s) nearby. During the freezing phase, a little bump is observed right before dropping because of water freezing. This bump gets wider as the sensor height is increasing, corresponding to liquid water pushed up by the frozen front. The 30-cm sensor is the last to be frozen and the first to be thawed.

Soil Freezing Characteristic Curves (SFCs) at different depths were determined from volumetric water content and temperature data collected during the experiment (Figure 2-d). No supercooling effect was observed as those observed in more complex soils (Ren and Vanapalli, 2020), neither a strong zero curtain effect. Hysteresis in the SFCs are observed for each depth due to air and/or water and/or ice entrapment.
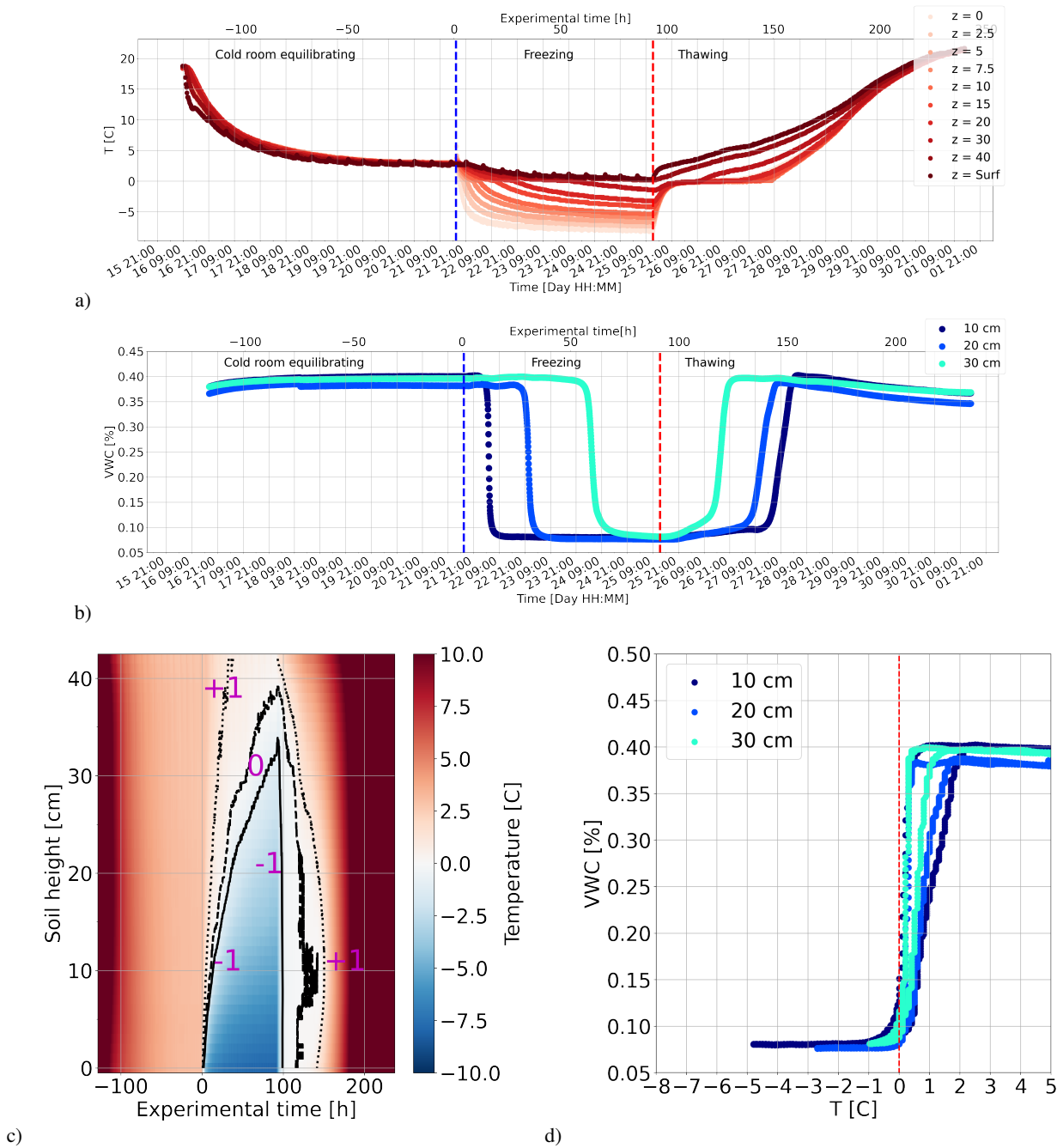
Figure 2. Temperature and volumetric water content monitoring of the experiment : a) thermal monitoring, b) volumetric water content monitoring, c) reconstructed 2D temperature column, d) soil freezing curves. Depth of the sensors are in centimeters from the base of the sand layer. Blue dashed line represents the start of the freezing phase, while the red dashed line represents the end of the freezing phase and the beginning of thawing.

3.2 M-GPR data

The simulated radargram is presented in Figure 3-a). As a recall, each trace has been computed from a dielectric permittivity distribution (derived from Equation 3) corresponding to a frozen layer increasing from 0.02 m up to 0.3 m with 2 cm step. They are presented Figure 3-b). The two-way travel-time of the reflection on the PEC layer (labelled A), represented as yellow crosses on Figure 3-a) has been computed from each permittivity distribution in the tank. Two reflections (B) and (C) are arriving earlier than reflection (A), directly linked to the frozen/thawed water saturated sand transition as seen in 3-b), where (A) is placed at the bottom of the tank, and points (B) and (C) are placed on sharp permittivity contrasts. We use this simple modeling to interpret the experimental radargram.

The experimental M-GPR radargram, presented Figure 3-c), displays three main reflections, labelled (A), (B) and (C). Comparing the experimental radargram to the simulated one, we find visual correspondences strengthening our assumption: the first (C) reflection corresponds to the frost table while the (B) reflection corresponds to the bottom of the transition zone, and (A) reflection to the aluminum PEC sheet. As opposed to the numerical case, (B) and (C) reflections are difficult to discriminate during the freezing phase, easier to distinguish during the thawing phase. The dynamic used in the numerical modeling (keeping a fixed transition zone thickness) does not fit the experimental data (where the transition thickness is clearly increasing with experiment time in Figure 2-c)). Beyond the reflection similitude, the amplitude and wavelet are different, mostly due to the different EM sources, the loss not taken into account in the modeling, the homogeneity and the isotropy, which are present in the experimental radargram.

These (B) and (C) reflections give us information on the thickness, the homogeneity and the dynamic of the active layer during the freezing and the thawing phases. We especially detect the speed of thawing being faster that the speed of freezing, and water redistribution in the near surface. In addition substracting the TWTs of these reflections (TWT_A-TWT_C) and comparing it with the $0°C$ isotherm height inferred from the thermistor time series (Figure 2-a) and-c)), gives the time needed for the electromagnetic wave to propagate through the frozen media as a function of its thickness. Figure 2-d) shows that the points (TWTs as a fonction of frozen front height) align in a linear relationship inversely proportional to the squared root of the bulk permittivity. By adjusting the linear regression with Theil Sen robust regression at 90% confidence interval we retrieve a bulk permittivity at $\varepsilon = 4.54 \pm 0.1$, similar to the literature for saturated frozen sand (Arcone et al., 1998).

4 Discussions, future works and conclusions

The M-GPR system has been capable to deliver the evolution of the thaw depth and the average soil water content between the surface and the freeze-thaw interface for the freezing and the thawing period. For the laboratory conditions encountered in the study, the M-GPR method was able to monitor a moving interface with an uncertainty being less than a centimeter, being sufficient to secure spatial differences in the thaw depth very small dynamic. The modeling presented in this study is very simple, but was aimed in understanding from where the reflections observed in the experimental radargram where coming from. A coupled thermo-hydro-EM modeling is currently in development in order to fully simulate the physical phenomena and use the M-GPR data to infer SFCs.
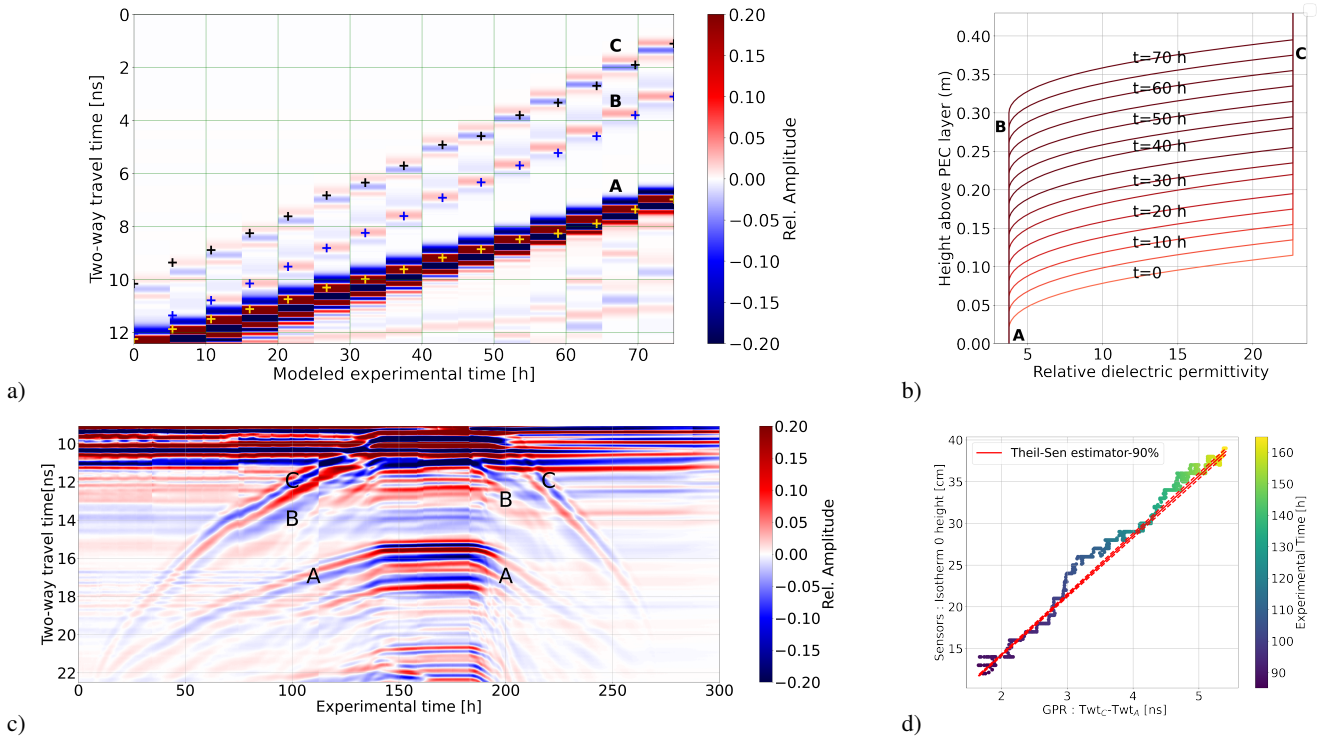
Figure 3. a) Simulated radargram with permittivity distributions shown in b). c) Experimental radargram displayed with normalized amplitude. Labelled (A), (B) and (C) reflections correspond to the permafrost base, bottom and top of the transition zone. Crosses in a) are computed TWT using permittivity distributions in b) where B and C positions are indicated for the $t = 65$ h. TWT stands for Two-Way travel Time. d) TWT_C and TWT_A difference as a function of $0°$C-isotherm height.

In terms of technical drawbacks, the main factors limiting the accuracy in the present study are: (1) the frost heave through the experiment and, (2) the surface condition changing the antenna impedance. The latter could be accounted for by using a bi-static antenna, allowing to retrieve the near surface hydric conditions and thus the impedance of the antenna. The first issue regarding the frost heave is easy to track in a laboratory experiment, here only 1-2 cm heave were observed since we used geotextile, while it is harder in the case of field studies. Beyond frost heave, soil tilting and surface de-planarization can happen and lead to loss of verticality and miscalculate the depth of the frost table.

The M-GPR system by its agility will be of use for better understanding the GPR reflection in the case of supra-permafrost water layer, especially if the reflection is due to the unsaturated soil/saturated soil interface and/or the freezing interface. This difficulty on what is actually reflected is illustrated by the difference in the modeling and the experimental radargram. As presented, the M-GPR system, is fully autonomous and can monitor during 2 month at 30 minutes intervals with a 12 V/60 Ah car battery without any recharge. The field deployment is about to start having been delayed due to international tensions. That

being said coupled with a set of temperature and volumetric water content, the method holds a strong potential for bringing

175 valuable thermo-hydro-dynamical information and refine the various processes taking place during melting and freezing.

References

Annan, A.: Ground Penetrating Radar: Workshop Notes, Tech. rep., Sensors and Software Inc., Ontario, Canada, 1999.

Arcone, S. A., Lawson, D. E., Delaney, A. J., Strasser, J. C., and Strasser, J. D.: Ground-penetrating radar reflection profiling of groundwater and bedrock in an area of discontinuous permafrost, Geophysics, 63, 1573–1584, 1998.

Birchak, J., Gardner, L., Hipp, J., and Victor, J.: High dielectric constant microwave probes for sensing soil moisture, Proceedings IEEE, 35, 85–94, 1974.

Costard, F., Dupeyrat, L., Séjourné, A., Bouchard, F., Fedorov, A., and Saint-Bézar, B.: Retrogressive Thaw Slumps on Ice-Rich Permafrost Under Degradation: Results From a Large-Scale Laboratory Simulation, Geophysical Research Letters, 48, e2020GL091 070, 2021.

Henry, K. S.: Laboratory investigation of the use of geotextiles to mitigate frost heave, Tech. rep., Cold regions research and engineering laboratory, Hanover, NH, 1990.

Hinzman, L. D., Goering, D. J., and Kane, D. L.: A distributed thermal model for calculating soil temperature profiles and depth of thaw in permafrost regions, Journal of Geophysical Research: Atmospheres, 103, 28 975–28 991, 1998.

Jadoon, K. Z., Weihermüller, L., McCabe, M. F., Moghadas, D., Vereecken, H., and Lambot, S.: Temporal monitoring of the soil freeze-thaw cycles over a snow-covered surface by using air-launched ground-penetrating radar, Remote sensing, 7, 12 041–12 056, 2015.

Léger, E., Saintenoy, A., Coquet, Y., Tucholka, P., and Zeyen, H.: Evaluating hydrodynamic parameters accounting for water retention hysteresis in a large sand column using surface GPR, Journal of Applied Geophysics, 182, 104 176, 2020.

Liu, L. and Arcone, S. A.: Numerical simulation of the wave-guide effect of the near-surface thin layer on radar wave propagation, Journal of Environmental & Engineering Geophysics, 8, 133–141, 2003.

Liu, X., Serhir, M., and Lambert, M.: Detectability of junctions of underground electrical cables with a ground penetrating radar: Electro-magnetic simulation and experimental measurements, Construction and Building Materials, 158, 1099–1110, 2018.

Mualem, Y.: A new model for predicting the hydraulic conductivity of unsaturated porous media., Water Resour. Res., 12, 513–522, 1976.

Ren, J. and Vanapalli, S. K.: Effect of freeze–thaw cycling on the soil-freezing characteristic curve of five Canadian soils, Vadose Zone Journal, 19, e20 039, 2020.

Saintenoy, A., Tucholka, P., Bailleul, J., Costard, F., Elie, F., and Labbeye, M.: Modeling and monitoring permafrost thawing in a controlled laboratory experiment, in: Proceedings of the 3rd International Workshop on Advanced Ground Penetrating Radar, pp. 79–83, 2005.

Steelman, C. M. and Endres, A. L.: Evolution of high-frequency ground-penetrating radar direct ground wave propagation during thin frozen soil layer development, Cold regions science and technology, 57, 116–122, 2009.

Sudakova, M., Sadurtdinov, M., Skvortsov, A., Tsarev, A., Malkova, G., Molokitina, N., and Romanovsky, V.: Using ground penetrating radar for permafrost monitoring from 2015–2017 at calm sites in the Pechora river delta, Remote Sensing, 13, 3271, 2021.

van der Kruk, J., Arcone, S. A., and Liu, L.: Fundamental and higher mode inversion of dispersed GPR waves propagating in an ice layer, IEEE Transactions on geoscience and remote sensing, 45, 2483–2491, 2007.

van der Kruk, J., Steelman, C., Endres, A., and Vereecken, H.: Dispersion inversion of electromagnetic pulse propagation within freezing and thawing soil waveguides, Geophysical Research Letters, 36, 2009.

van Genuchten, M. T.: A Closed form equation for predicting the hydraulic conductivity of unsaturated soils, Soil Sci. Soc. Am. J., 44, 892–898, 1980.

Warren, C., Giannopoulos, A., and Giannakis, I.: gprMax: Open source software to simulate electromagnetic wave propagation for Ground Penetrating Radar, Computer Physics Communications, 209, 163–170, 2016.

Westermann, S., Wollschläger, U., and Boike, J.: Monitoring of active layer dynamics at a permafrost site on Svalbard using multi-channel ground-penetrating radar, The Cryosphere, 4, 475–487, 2010.

215 *Acknowledgements.* This study has been funded by the Instrumentation in situ en conditions extrêmes - AAP 2020 MITI SUPERLEVELING project INSU.

Critical reviews by Adam Booth and an anonymous reviewer greatly enhanced the presentation of this manuscript.

This article is dedicated to Christophe Grenier.